

## Development and Study of a Portable Plasma Focus Neutron Source

V. P. Vinogradov<sup>a</sup>, A. V. Nashilevskii<sup>b</sup>, V. I. Krauz<sup>a</sup>, G. E. Remnev<sup>b</sup>, Yu. V. Vinogradova<sup>a</sup>,  
G. G. Kanaev<sup>b</sup>, K. N. Mitrofanov<sup>c</sup>, and V. V. Myalton<sup>a</sup>

<sup>a</sup> National Research Centre Kurchatov Institute, pl. Akademika Kurchatova 1, Moscow, 123182 Russia

<sup>b</sup> National Research Tomsk Polytechnic University, pr. Lenina 30, Tomsk, 634050 Russia

<sup>c</sup> Troitsk Institute for Innovation and Fusion Research, Troitsk, Moscow, 142190 Russia

e-mail: krauz@nfi.kiae.ru

Received August 22, 2013

**Abstract**—The work is devoted to designing a compact pulsed neutron source on the basis of a plasma focus (PF) discharge. The main task was to study the physical processes accompanying a sub-kilojoule repetitive PF discharge. A device with a power supply energy of up to 600 J and pulse repetition rate of up to 10 Hz has been developed and put into operation. The dependence of the neutron yield as a function of the pulse repetition rate has been studied experimentally. A neutron flux of  $\sim 10^8$  neutrons/s has been obtained in the 3-s-long packet mode with a repetition rate of 10 Hz and discharge current of 80–90 kA.

**DOI:** 10.1134/S1063780X1402007X

### 1. INTRODUCTION

It is well known that the emission parameters of a plasma focus (PF) device depend strongly on the discharge energy. In particular, in a wide range of the power supply energies, the neutron yield increases quadratically with increasing discharge energy. Among the wide variety of PF devices, three main groups differing in the power supply energies can be distinguished. The best studied group is devices with supply energies from several to a few hundred kilojoules (see [1, 2]). It is for this group of devices that the well-known experimental scaling  $N \sim W^2$  was obtained [3]. The next class of devices appeared as a natural consequence of this scaling. Those are devices with stored energies on the order of 1 MJ. At present, there are four devices operating in this energy range: PF-3 (National Research Centre Kurchatov Institute, Moscow, Russia,  $W_{\max} = 2.7$  MJ,  $T/4 = 20$   $\mu$ s,  $I = 2$ –5 MA) [4], PF-1000 (Institute of Plasma Physics and Laser Microfusion, Warsaw, Poland,  $W_{\max} = 1.06$  MJ,  $T/4 = 6$   $\mu$ s,  $I = 2$  MA) [5], KPF-4 Phoenix (Sukhum Institute of Physics and Technology, Sukhum, Abkhazia,  $W_{\max} = 1.8$  MJ,  $T/4 = 8$   $\mu$ s,  $I = 2$ –3.5 MA) [6], and GEMINI (NSTec, Las Vegas, United States,  $W_{\max} = 1$  MJ,  $I = 3$ –4 MA) [7]. These devices are mainly intended to confirm the scaling in the 1-MJ energy range and achieve a D–D neutron yield of  $\geq 10^{13}$  neutrons/shot. Such devices are small in number because of their high cost, and the desired goals have not been reached as of yet.

Since recently, PF devices with sub-kilojoule power sources began to be actively developed. Such devices

are aimed at a wide spectrum of practical applications: EUV lithography, detection of explosives, radiation medicine, radiation material science, production of new nanostructured coatings, and others [8–20]. The main requirements to such devices are the high emissivity when operating in a repetitive mode, reproducibility, compactness, the high conversion efficiency of the energy stored in the capacitor bank into radiation, etc. In particular, in order to reduce the sample irradiation nonuniformity caused by the scatter in the emission parameters from shot to shot, it is necessary that the device operates in the repetitive mode, which limits the discharge energy. For example, for the well-studied devices with a stored energy of a few kilojoules and a repetition rate of 1 Hz, the consumed power is a few kW. Many practical applications require a higher pulse repetition rate: a few tens or hundreds of Hz (and even a few kHz for the needs of EUV lithography). It is clear that, in order to keep the power consumption in reasonable limits, it is necessary to reduce the energy of individual shots. In this case, one has to search for the optimum between the discharge energy (the lower the energy, the lower the radiation yield) and the pulse repetition rate. In spite of the effort made in recent years on studying various scalings in this energy range, including the neutron scaling [21], this problem is far from being resolved. The available literature data show that the attained emission parameters vary in a wide range (by an order of magnitude and more). The situation becomes even more unclear when the device operates in the repetitive mode.

At present, experiments with kilojoule and sub-kilojoule devices are the most actively developed lines

of PF research. In particular, active studies in this direction are being carried out in Chile, where several devices operating in this energy range have been created. For example, a  $10^6$  neutron yield was obtained at the PF-400J device (880 nF, 38 nH, 20–35 kV, 176–539 J) at a discharge current of 127 kA [22]. A neutron yield of  $4 \times 10^4$  neutrons/shot was obtained at the PF-50J device (160 nF, 38 nH, 20–30 kV, 32–72 J) at a discharge energy of 67 kJ [23]. Recently, it was reported on the creation of a subminiature PF device with an energy of 60–250 mJ [24, 25], at which X-ray emission was detected at a discharge energy as low as 0.1 J and a neutron yield of  $\sim 10^2$  neutrons/shot was obtained.

Similar studies are being actively developed at the Nanyang Technological University (Singapore). At the FMPF-1 device (2.4  $\mu$ F, 27 nH,  $T/4 \sim 400$  ns, 12–15 kV, 170–270 J), a neutron yield of  $\sim 10^4$  neutrons/shot was obtained at a current of 70 kA [26]. Similar experiments are being conducted in Russia (PF-0.2, 200 J [27]), Argentina, India, and other countries. One of the best results was obtained at the Nanofocus device [28], where a neutron yield of  $10^6$  neutrons/shot was achieved at a power supply energy as low as 125 J.

In almost all of the above-cited works, it was emphasized that, in order for the device to be used for practical applications, it should operate in the repetitive mode. However, publications concerned with this problem are very scarce. For example, devices with energies at a level of a few kilojoules operated in the repetitive mode. At a device operating for 3–5 min with a discharge energy of 4.7 kJ and pulse repetition rate of 0.2 Hz, the mean neutron yield of  $10^8$  neutrons/pulse was obtained over only the first 20 pulses, after which the neutron yield degraded [29]. The NX1 and NX2 devices (Singapore,  $W \sim 2$  kJ, the discharge current of up to 400 kA) are intended to operate at a higher repetition rate (up to 16 Hz) [30].

Information concerning the repetitive mode of PF operation in the sub-kilojoule energy range appeared relatively recently. Here, the works by the CYMER corporation (United States) are worth being specially mentioned. In those works, a PF device operating in the packet mode with a repetition rate up to 2 kHz and discharge energy in individual pulses of a few joules was developed for lithography purposes [12]. However, this device was not tested in the neutron generation mode. The best results in the development of a neutron source operating in the repetitive mode were obtained in the experiments carried out at the FMPF-2 and FMPF-3 devices [31, 32], where a neutron flux of  $(1.4 \pm 0.2) \times 10^7$  neutrons/s was achieved at a repetition rate of 10 Hz, discharge energy of 200 J, and discharge current of 103 kA.

At the same time, for a number of practical applications, e.g., signature-based radiation scanning (SBRs) using combined photon and neutron interro-

gation for homeland security applications, neutron fluxes of  $\geq 10^8$  neutron/s are required [32].

The aim of the present work was to study and optimize the emission characteristics of a sub-kilojoule PF operating in the repetitive mode.

To solve this problem, a new PF device has been developed and put into operation. The work involved three main stages:

- (i) the development of the optimal PF design,
- (ii) the creation of a power source providing a pulsed current of  $\sim 100$  kA through the load at a pulse repetition rate of up to 10 Hz, and
- (iii) the study of the dynamics and emission characteristics of the discharge in both the single-pulse and repetitive modes.

## 2. DEVELOPMENT OF THE OPTIMAL DESIGN OF THE DISCHARGE SYSTEM BY USING A PROTOTYPE POWER SOURCE OPERATING IN THE SINGLE-PULSE MODE

Since the physics of a discharge operating in the repetitive mode is poorly understood, the main objective of the first stage was to develop the design and search for optimal conditions in the single-pulse mode. The optimal design of the discharge system was developed using a prototype power source. As a capacitance bank, we used a 2.7- $\mu$ F IK50-3 capacitor with the maximum charging voltage of 50 kV. The switching element was a three-electrode spark gap operating at atmospheric pressure. The maximum charging voltage was determined by the interelectrode distance; in our experiments, it did not exceed 24 kV, which corresponded to the stored energy of 800 J. The insulation of the electrode system was also designed for this voltage. Most experiments were carried out at a charging voltage of 20 kV (540 J).

In order to reduce the inductance, the spark gap and the PF chamber were mounted directly on the capacitor by means of feed bars. The measured total inductance of the prototype power source assembled with the discharge chamber was 112 nH, which, in a lossless circuit, would make it possible to obtain a discharge current pulse with an amplitude of up to 100 kA and a rise time of  $\leq 1$   $\mu$ s at a voltage of 20 kV. Due to losses in the capacitor, spark gap, and PF load, as well as to the variable inductance of the PF load, the actual amplitude of the current pulse did not exceed 75 kA.

A 20-kV ignition voltage pulse was supplied to the middle (control) electrode of the spark gap through a 5-m-long RK-75-4 cable. As a result of voltage doubling, a pulse with an amplitude of 40 kV and a duration of 50 ns formed at the open end of the cable.

Using this prototype power source, eight versions of the discharge system were tested. In the first stage, a discharge system with a 20-mm-diameter porcelain insulator was used. In these experiments, the cathode had the form of a squirrel cage made of 12 6-mm-

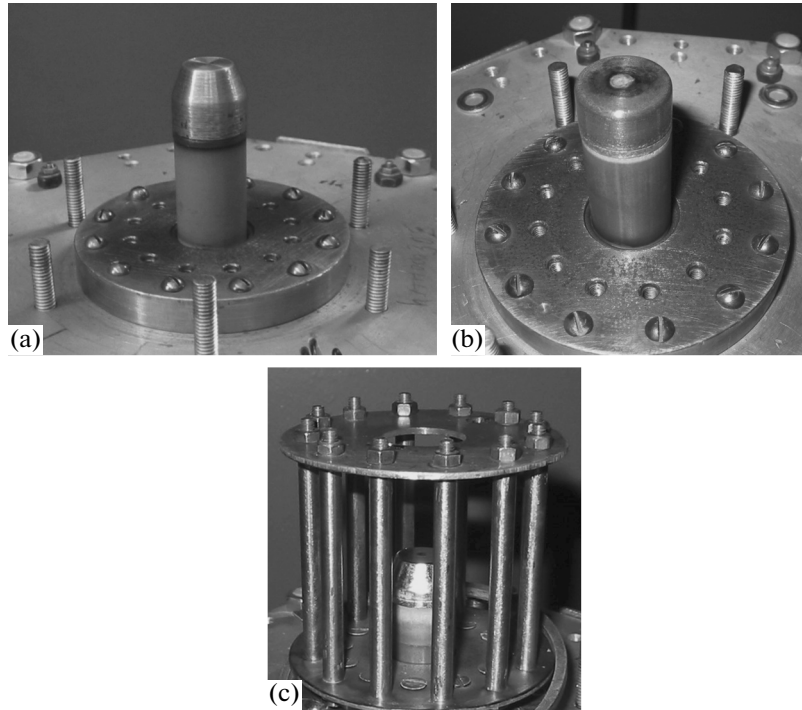


**Fig. 1.** Photographs of (a, b) different versions of the anode unit with a 20-mm-diameter insulator and (c) the assembled discharge system.

diameter copper rods installed at a radius of 32 mm. The anode had the same diameter as the insulator, and the anode–insulator joint was flush-mounted. The relatively large anode diameter was dictated by the necessity of its cooling when operating in the repetitive mode. Several versions with different lengths of the insulator (from 10 to 30 mm) and anode (from 5 to 30 mm) and different shapes of the anode were tested. Several versions of the transition from the cylindrical part of the anode near the insulator to the truncated conical part with different cone angles and a plane end face were studied. Photographs of some versions of such a discharge system are shown in Fig. 1.

Along with radiative characteristics, one of the main criteria of the discharge quality is the presence of a sharp dip (singularity) in the current time derivative  $dI/dt$ , which indicates the high compression ratio of the current and the formation of a pinch on the axis. To achieve the required operating mode, it is usually necessary to train the chamber and the electrode system, in particular, to clean the insulator surface from impurities. The duration of training is determined by the discharge energy and the area and state of the insulator surface. Therefore, Filippov-type systems, in which the diameter of the discharge system is larger than its length, require a longer training than the Mather-type systems with the same discharge energy. Since the described version of the discharge system was similar to a Filippov-type system and the discharge energy was relatively low ( $\sim 500$  J), a few hun-

dred training pulses were needed to reach the required operating regime.

In the beginning of the training series, several discharges were performed in the chamber filled with krypton at a pressure of 5 Torr. At such a high pressure, the plasma current sheath (PCS) had no time to move away to a significant distance from the insulator. This allowed us to determine the initial (minimal) inductance of the discharge circuit, which was found to be 112 nH, the damping constant being 0.43–0.52. The time derivative  $dI/dt$  increased from zero to its maximum value for about 200 ns and was small in amplitude (less than or equal to the first minimum).

It is well known that the main principle of matching the discharge system to the power source is to reach focusing (pinch formation) near the first maximum of the discharge current. Unfortunately, we failed to achieve such a discharge regime for all versions of the discharge system with an insulator diameter of 20 mm in the entire range of the working gas ( $D_2$ , Kr, Ne) pressures under study (from several to 20 Torr). In the best case, a weak singularity in the current time derivative was observed only at the end of the first half-period of the discharge current, i.e., when the discharge current was practically zero (Fig. 2a). We succeeded to obtain a sufficiently pronounced dip in the current time derivative only in the third half-period of the discharge current (Fig. 2b) when operating with heavy gases. Accordingly, the detectors calibrated in the actual geometry of our experiment and

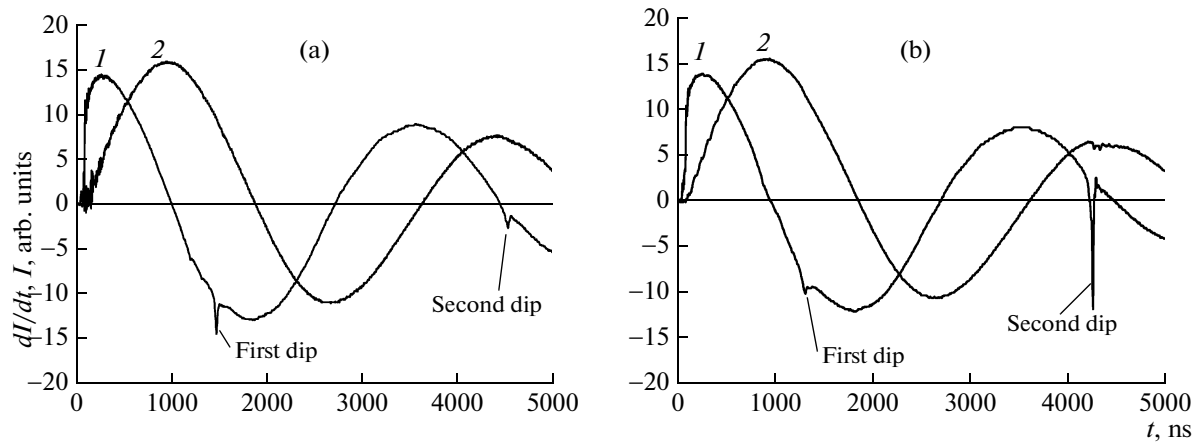


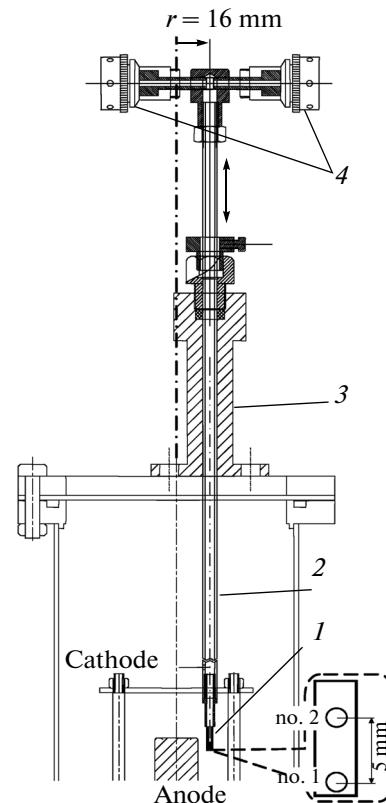
**Fig. 2.** Waveforms of the discharge current (curve 2) and its time derivative (curve 1) in a discharge system with a 20-mm-diameter insulator ( $W = 540$  J,  $V = 20$  kV) operating with different working gases: (a) deuterium at 6 Torr and (b) krypton at 1 Torr.

having a sensitivity of  $3 \times 10^4$  neutrons/count did not detect any neutron emission.

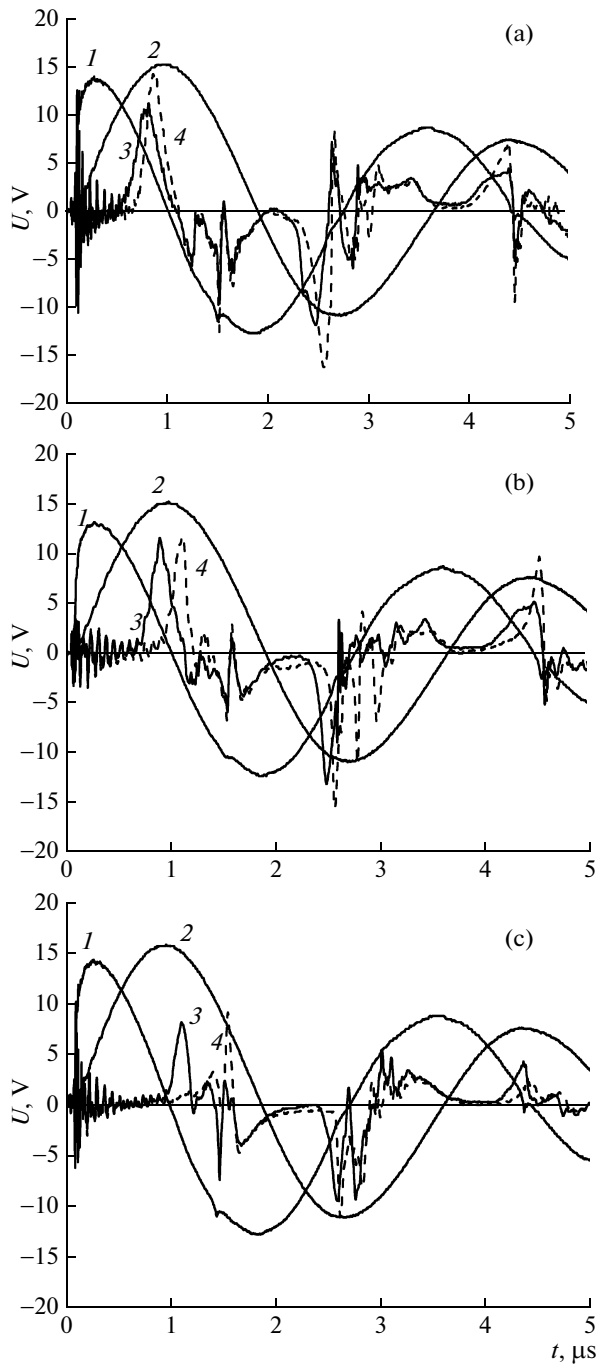
The absence of matching can be caused by the late arrival of the PCS at the electrode end, current leakage near the insulator, and other reasons. The current carried away by the PCS to the anode end was measured by magnetic probes consisting of two  $\sim 800$ - $\mu\text{m}$ -diameter four-turn coils placed at a distance of  $\sim 5$  mm from one another on the axis of a ceramic tube. The sensitivity of the probes was 270 V ns/kG. Each coil measured the rate of change of the azimuthal magnetic field (the time derivative of the magnetic induction) at the point of its location. The current pulse waveform was recovered by numerically integrating the probe signal under the assumption that the current-carrying plasma was axisymmetric. In this manner, we calculated the current flowing within the radius at which the probe was placed. The probe holder made it possible to install the probe at a distance of 16 mm from the chamber axis and move it along the axis without violating the vacuum conditions. The scheme of measurements is shown in Fig. 3.

Figure 4 shows typical signals from probes placed in the electrode gap at the radius of 16 mm at different distances from the anode end. We observed a time delay in the appearance of signals from two probe coils, from which we could estimate the PCS propagation velocity along the accelerating channel. For the probe position in which the first coil was at a distance of  $-10$  mm from the anode end (inside the acceleration channel), this velocity was  $\sim 5 \times 10^6$  cm/s. Closer to the anode end, the time delay increases, which may be caused by the deceleration of the PCS due to an increase in its mass at nearly the same discharge current (for the probes positioned at  $-10$  and  $-5$  mm; see Figs. 4a, 4b). For the probe positioned at 0 mm (Fig. 4c), the time delay can also increase due to an appreciable decrease in the discharge current in this stage of PCS motion. Moreover, it is also necessary to

take into account a possible change in the PCS shape (the slope angle), especially in the stage in which the PCS moves along the conical part of the anode, as well as in the stage of radial compression. The probe placed



**Fig. 3.** Scheme of magnetic probe measurements inside the PF chamber: (1) two-loop sensitive element, (2) 6-mm-diameter vacuum-tight steel tube, (3) vacuum lock, and (4) coaxial connectors. The inset shows the arrangement of coil nos. 1 and 2 inside the sensitive element.



**Fig. 4.** Waveforms of the total current (curve 2), its time derivative (curve 1), and signals from two magnetic probe coils separated by a distance of 5 mm (curves 3, 4). The first coil is inside the electrode gap at a distance of (a)  $-10$  and (b)  $-5$  mm from anode end and (c) flush with the anode end.

aflush with the anode end is approached by the PCS practically at the instant of pinching on the axis.

We observed the arrivals of several PCSs in each half-period of the discharge current. In this case, the arrival of the PCS in the second half-period (in which

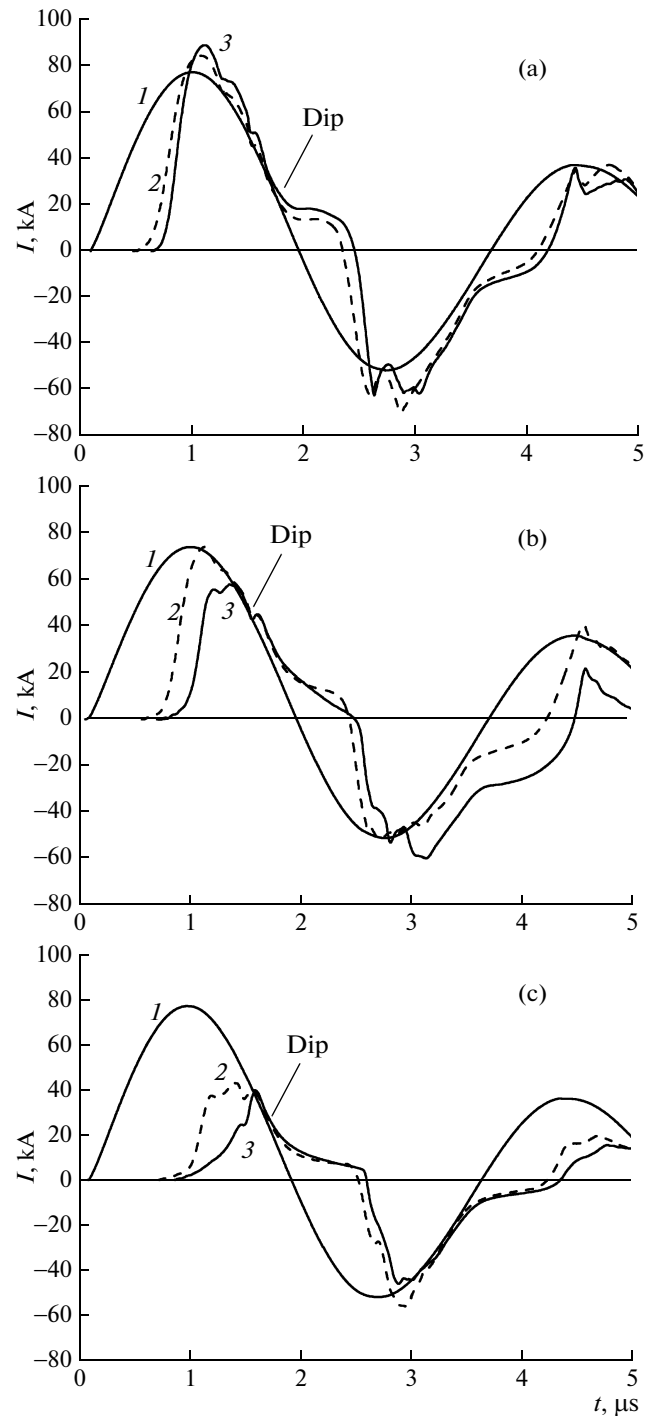


**Fig. 5.** Waveforms of the total current measured by the Rogowski coil (curve 1) and currents obtained by integration of magnetic probe signals for the pulses presented in Fig. 4 (curves 2, 3). The positions of the probes with respect to the plane of the anode end are (a)  $-10$ , (b)  $-5$ , and (c)  $0$  mm.

the polarity of the central anode was negative) was not accompanied by the appearance of a sharp dip in the current time derivative, although the instant of pinching practically coincided with the current maximum.

At the same time, the PCS compression in the third half-period resulted in the appearance of such a dip, the magnitude of which was often higher than in the first half-period (Fig. 2b).

Figure 5 shows waveforms of the current flowing within the radius at which the probe was installed. It should be noted that, after the PCS has passed the probe, the current measured by the probe coincides to within measurement errors with the total discharge current, i.e., the current is efficiently snowplowed toward the axis. At the same time, it is seen that the maximum of the total current is reached before the PCS approaches the anode end, i.e., the pinching takes place at a sufficiently low current, which manifests itself in a weakly pronounced singularity in the time derivative of the total current. At discharge currents below 75 kA, which are attainable on the prototype power source, we failed to improve the matching of the load to the parameters of the power source by varying the anode length or the working gas pressure. Apparently, for a relatively large insulator diameter, the formation of the PCS near the insulator takes too much time as compared to the time of its accelerated motion. Therefore, we failed to improve matching by reducing the electrode length or increasing the working gas pressure, because, for the remaining time, the PCS cannot reach the axis up to the instant corresponding to the maximum of the discharge current. Obviously, in order to reduce the PCS formation time, it is necessary to increase the current growth rate in the beginning of the discharge. In our opinion, this explains the difference from the results of [33], where  $\sim 10^7$  neutrons/shot were obtained in a system with an anode diameter of 20 mm and a discharge current of 120–140 kA.

It also follows from Fig. 5 that, some time after PCS compression on the axis (the dip in the current time derivative), the current measured by the probes becomes directed oppositely to the total current. This indicates the development of a secondary breakdown, most probably, near the insulator. In this case, a new PCS forms near the insulator and the probe detects the magnetic field inside a certain closed current formation arising near the anode end. After the arrival of the second PCS, the direction of the current detected by the probe changes abruptly and coincides again with the direction of the total current. A similar effect is also observed in the third half-period of the discharge current.

It should be noted that the occurrence of several pinches in different half-periods of the discharge is typical of small PF devices [34, 35].

The observed phenomena can be interpreted as follows. After the development of the secondary breakdown, the discharge current begins to flow along the insulator surface. In this case, a fraction of the magnetic flux produced by the current flowing in the PCS is switched off and a new closed circuit forms. The

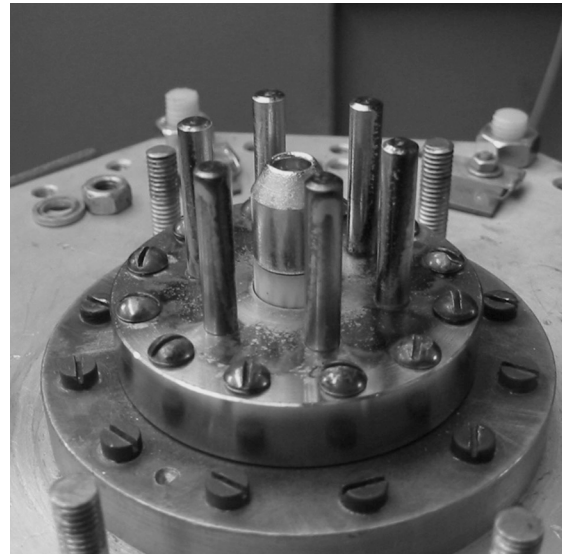
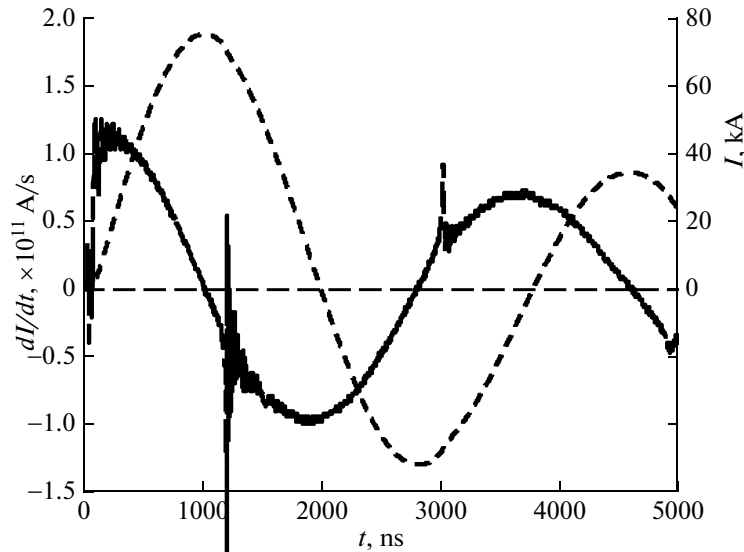


Fig. 6. Photograph of the discharge system with a 12-mm-diameter insulator.

current flowing in this circuit continues to form a typical PF with a contraction on the axis in front of the anode end. A similar effect was previously observed at the PF-3 device at discharge currents of  $\sim 2$  MA [36, 37].

The probe signals from both coils exhibit a typical sharp dip, which is almost imperceptible in signals from the magnetic probe and the Rogowski coil placed outside the discharge chamber, because field variations inside a separate current vortex are screened by the current flowing along the insulator surface. Nevertheless, current contraction takes place, which is indicated by the formation of an appreciable melting with a diameter about 3 mm at the center of the anode end, which is clearly seen in the anode photograph made after a long series of discharges (Fig. 1b).

The results improved substantially only after the insulator and anode diameters were reduced from 20 to 12 mm, which led to an increase in the current density in the PCS in the stage of its formation. A similar system was used in [31, 32]. A stainless-steel or copper anode with a length of 15 mm had a cylindrical part with a length of 10 mm and diameter of 12 mm, equal to the diameter of the 6-mm-long alundum insulator, and a conical section with a length of 5 mm. The diameter of the hollow anode end was 6 mm, the depth of the hollow being 12 mm. The cathode was made of six 6-mm-diameter stainless-steel rods installed at the radius of 15 mm. Figure 6 shows the photograph of such an electrode system after a long series of discharges. It is worth noting strong melting of the anode end, which indicates efficient transportation of the current to the anode end. After modifying the electrode system, the number of discharges required to achieve the operating regime decreased to  $\sim 50$ . A pro-



**Fig. 7.** Waveforms of the total discharge current (dashed curve) and its time derivative (solid curve) recorded in experiments with a discharge system with a 12-mm-diameter insulator.

nounced dip in the current time derivative near the maximum of the discharge current is observed (Fig. 7). A certain time delay with respect to the current maximum can be attributed to both the nonoptimal matching and a decrease in the current caused by a sharp increase in the discharge circuit inductance in the final stage of PCS radial compression [38]. It should be noted that the second compression is observed in the second half-period of the discharge current, i.e., at the negative polarity of the central electrode, which agrees with the above-described secondary breakdown and the formation of the second PCS. Nevertheless, in this regime, the formation of the first PCS is already accompanied by efficient pinching, which, in particular, manifests itself in an increase of the neutron yield.

### 3. STUDY OF THE PARAMETERS OF NEUTRON AND X-RAY EMISSION AT THE PROTOTYPE MODEL OF THE GENERATOR

The integral neutron yield was measured by an activation detector consisting of a Geiger counter covered with a silver foil and a polyethylene moderator calibrated by means of two neutron sources: an ING-12 pulsed neutron source and a stationary PuBe source. Calibration was performed in the actual experimental geometry by installing the source in the vacuum chamber at the place of PF formation, which made it possible to take into account the influence of the scattered neutron background. In the experiments described below, the number of detector counts exceeded the background level by more than one order of magnitude. The maximum detected neutron yield

in the experiments with the prototype model of the generator was  $\sim 8 \times 10^6$  neutrons/shot.

To perform time-resolved measurements of neutron emission and hard X-ray (HXR) emission with photon energies above 20 keV, we used two SNFT-3 photomultiplier tubes (PMTs) with 50-mm-diameter 100-mm-long plastic scintillators.

It was expected that, due to the small electrode dimensions and short discharge duration, the X-ray and neutron pulses at the given device will be as short as several tens of nanoseconds. Therefore, special attention was paid to testing the time characteristics of the PMTs. Although SNFT-3 PMTs are fairly fast, they have an appreciable time delay (dead time) between the input optical and output electric signals. According to [39], this time delay depends on the PMT power supply voltage and, for an SNFT PMT operating at a voltage of 4000 V, is  $\approx 43$  ns. Our experiments with two PMTs placed at equal distances (30 cm) from the PF showed that the dead times of the PMTs differed by  $\approx 3$  ns, which should be taken into account when interpreting the recorded signals. In addition, it was found that the amplifications of two identical PMTs operating at the same voltage of 4000 V differed by a factor of 8. This difference turned out to be useful for experiments in which the PMTs were installed at different distances from the emission source.

Figure 8 shows signals from PMT no. 1, placed at a distance of 30 cm, and PMT no. 2, placed at a distance of 100 cm. In this experiment, the PMT scintillators were protected from X-rays only by the 1-mm-thick aluminum cases of the PMTs and the 3-mm-thick wall of the discharge chamber.

In the PMT signals, we clearly see X-rays pulses, as well as neutron pulses delayed by the time of flight. The observed shift between the X-ray pulses ( $\approx 5$  ns) is caused by the difference in the times required for photons to travel different distances ( $\approx 2.3$  ns) and the above-mentioned difference in the PMT dead times. For a distance of 100 cm, the difference in the times of flight turned out to be sufficient for reliable separation of X-rays and neutrons. The time delay between X-ray and neutron pulses is in good agreement with the time of flight of neutrons with energies of about 2.5 MeV. More accurate measurements will be presented below when describing device operation in the repetitive mode.

In order to separate out purely neutron radiation, the scintillation detectors were additionally protected from HXR emission by 4-mm thick lead screens. Figure 9 shows typical neutron pulses obtained under these experimental conditions. In this regime, we usually observed discharges with two dips in the current time derivative, separated in time by about 100 ns, each of which could be accompanied by neutron emission (Fig. 9a). Probably, the PCS initially has a double-shell structure. In this case, the neutron intensity in each pulse depends on the distribution of the current between these shells. Sometimes, discharges are observed in which the first shell carries only a small fraction of the total current, which is expressed in a relatively small dip. In this case, the first compression is not accompanied by neutron emission and the neutron yield takes place only during the second compression (Fig. 9b). It should be noted that, in the latter case, the full width at half-maximum of the neutron pulse did not exceed 10 ns, which is rather important for some practical applications.

It is also worth noting that regimes with two compressions are typical of discharge systems with a hollow anode end. For an anode with a solid end, regimes with a single compression are typical. It may be supposed that the shape of the anode end affects the pinching dynamics in such a way that, in the case of a hollow anode, the first pinching takes place on the axis in front of the anode end, while the second pinching occurs inside the hollow after the PCS reaches the bottom of the hollow. For the PCS velocity of  $\geq 10^7$  cm/s and the anode hollow depth of 1.2 cm, the time during which the PCS moves from the anode end to the bottom of the hollow is  $\sim 100$  ns, which agrees with the observed time delay between two neutron pulses.

#### 4. DEVELOPMENT OF THE REPETITIVE HIGH-VOLTAGE GENERATOR

The final goal of this work was to implement the repetitive mode of PF operation in the sub-kilojoule range of discharge energies. In order to reach this goal, a low-inductive high-current pulsed generator (HCPG) capable of operating with a repetition rate of up to 10 Hz was developed on the basis of a pulsed

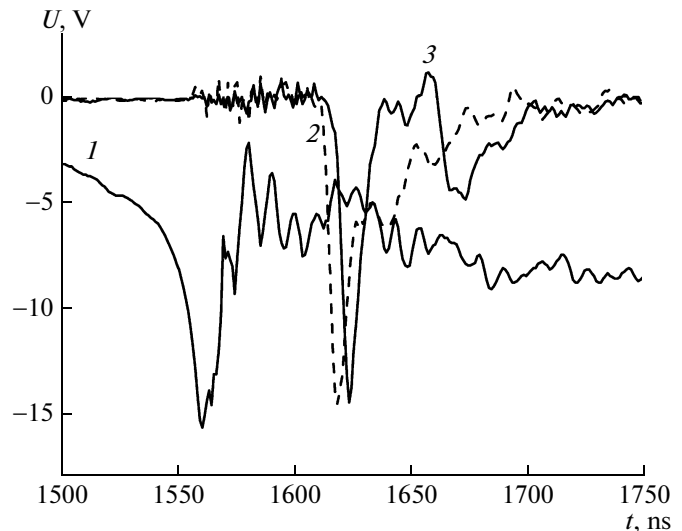
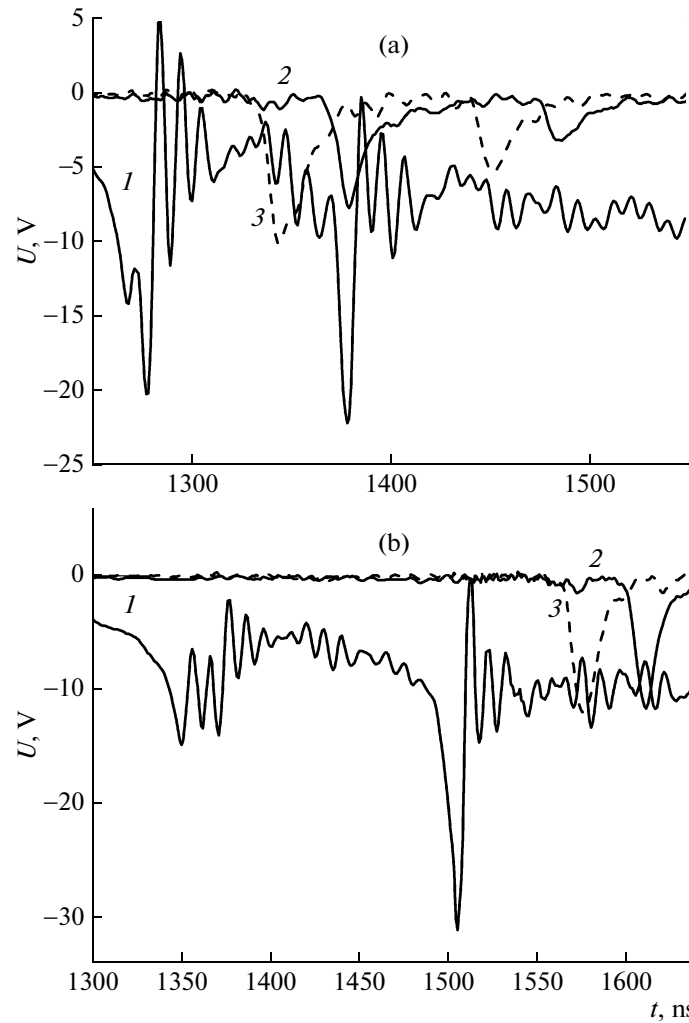


Fig. 8. Signals from scintillation detectors placed at distances of 30 cm (PMT no. 1, curve 2) and 100 cm (PMT no. 2, curve 3) from the pinch and waveform of the current time derivative (curve 1).

transformer [40, 41]. The HCPG electric circuit is presented in Fig. 10. Capacitor  $C$  is charged from a pulsed power source through the primary coil of the pulse transformer (PT). In this case, the PT core is demagnetized by the charging current. At the instant at which capacitor  $C$  is charged to the maximum voltage, the triggering voltage pulse is supplied to the multichannel switch (MS), after which capacitor  $C$  discharges through the MS and the primary coil of the PT. The voltage produced in the secondary coil of the PT is applied to the PF electrodes. The total current  $I_0$  was detected by a Rogowski coil (RogC). The generator was adjusted to operate in the repetitive mode with an equivalent load in the form of parallel copper buses. The discharge of the low-inductive HCPG through the equivalent load was rather stable, the maximum discharge current  $I_{\max}$  at a charging voltage of 40 kV being 74 kA. At repetition rates below 1 Hz, the scatter in the maximum generated current was as low as  $\pm 2\%$ . However, at higher repetition rates, the MS operation became unstable.

In order to test whether the PF device can be fed from the HCPG, the PF chamber with the optimal version of the electrode system developed using the prototype model of the generator was connected to the output flange of the HCPG (Fig. 11). In test experiments, neon was used as the working gas. Regimes with PF formation were obtained, which manifested itself in the appearance of a dip in the current time derivative. Figure 12 shows typical waveforms of the discharge current and its time derivative in the single-pulse mode. It is worth noting that, due to the low inductance of the HCPG, the amplitude and growth rate of the discharge current obtained with this power



**Fig. 9.** Waveforms of the time derivative of the total current (curve 1) and neutron signals recorded by PMT no. 2 (curve 2) and PMT no. 1 (curve 3) in the regime with two compressions.

source were somewhat higher than those in the case of the prototype model of the generator. Such current pulses were observed in series of up to 55 discharges at

pressures of 10–20 Torr without gas refreshing. The stability of PF operation can be illustrated by a series of 37 discharges performed during 9 min at a pressure of 10 Torr. In most of these discharges, the depth of the dip in the current time derivative varied by no more than 20%.

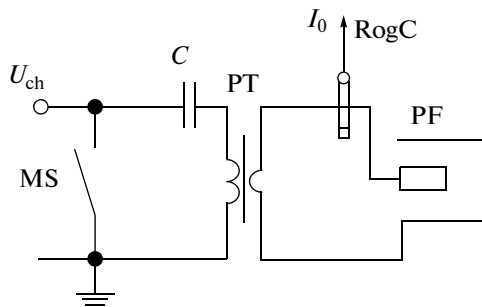


**Fig. 10.** Electric circuit of the experiment with a low-inductance pulsed high-current generator with a transformer output and PF load.

These parameters persisted when the generator operated at repetition rates of up to 1 Hz. However, as was noticed above, at repetition rates of 1–10 Hz, the MS operation became unstable due to the heating of its working gas ( $N_2$ ) and its electrodes. Special measures undertaken for heat removal from the MS (water cooling of the MS lid and gas circulation) provided stable operation of the generator only for a few seconds. Then, the amplitude of the charging voltage and, accordingly, the load current decreased appreciably. In order to decrease scatter in the output parameters to 2–5% at repetition rates of up to 10 Hz, the eight-channel gas spark gap was replaced with a TD14-100k/45PD hollow-anode thyatron. The thyatron

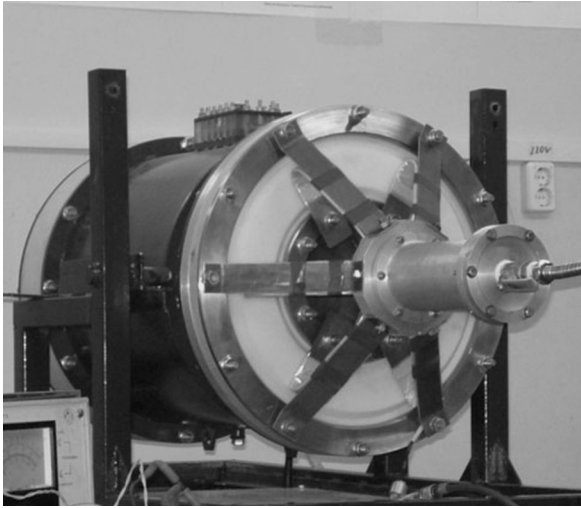


**Fig. 11.** Photograph of the generator assembled with the PF chamber.

has a metal–ceramic case and, in the working state, is filled with the buffer gas (hydrogen) at a pressure of 20–60 Pa. To ensure its cooling, the thyatron was placed inside the pulse transformer case filled with transformer oil. The use of this thyatron makes it possible, in principle, to increase the repetition rate to 200 Hz.

After upgrading, the generator provided PF operation at a repetition rate of 10 Hz, the scatter in the output voltage being 1–2%.

## 5. STUDY OF THE EMISSION PARAMETERS OF THE PF DEVICE OPERATING IN THE REPETITIVE MODE

In the experiments performed with the use of the HCPG, the parameters of the discharge system were somewhat modified. The diameters of the anode and aluminum insulator were increased to 14 mm, and 12 4-mm-diameter rods were used as the cathode. The emission parameters in the repetitive mode were studied using two methods: the detection of the neutron yield by means of an activation detector and time-resolved measurements of neutron and X-ray emission by means of a scintillation detector. Figure 13 shows waveform of the current time derivative and the signal from the radiation detector consisting of a polystyrene scintillator and an SNFT-3 PMT. The first and second peaks in the PMT signal correspond to HXR and neutron emission, respectively. Analysis of the signals indicates the presence of intense HXR emission with photon energies of  $>20$  keV. The integral yield of HXR emission was estimated by means of dosimeters. In a series of 14 shots, a 300-mR HXR dose was detected behind a 3-mm-thick duralumin screen on the side wall of the PF chamber at a distance of 50 mm from anode end.

If the PMT with the scintillator is placed in its standard 1-mm-thick duralumin case, then the amplitude of the HXR signal substantially exceeds the amplitude of the neutron signal. In order to reduce the HXR signal, the scintillator and the PMT case were additionally covered by a 3-mm-thick lead sheet, so that only photons with energies above 200 keV could reach the scintillator. As a result, not every neutron pulse was

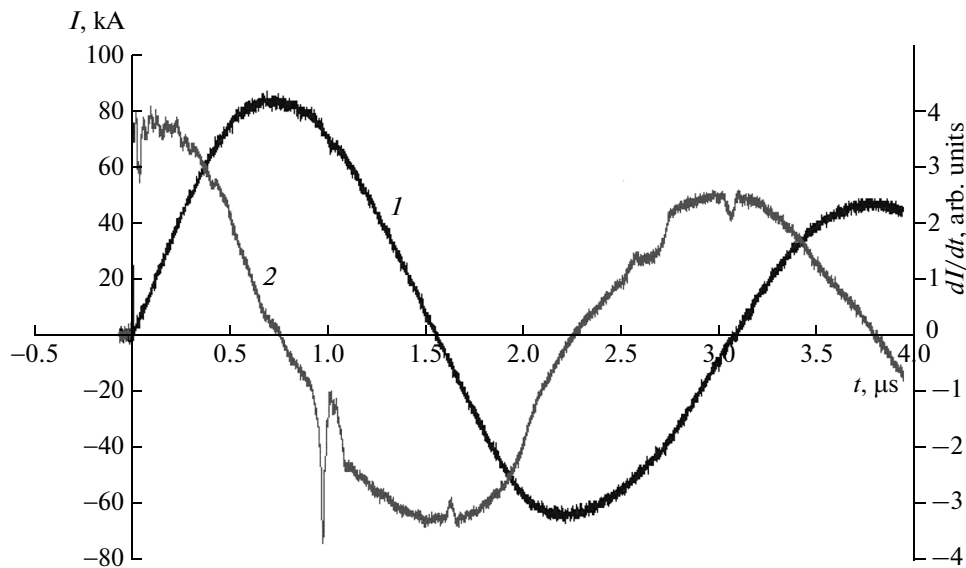


**Fig. 12.** Waveforms of the discharge current ( $I$ ) and its time derivative ( $2$ ) recorded in a PF discharge fed from a generator with a transformer output in the single-pulse mode ( $D_2$ , 13 Torr,  $V = 32$  kV, and  $W = 512$  J).

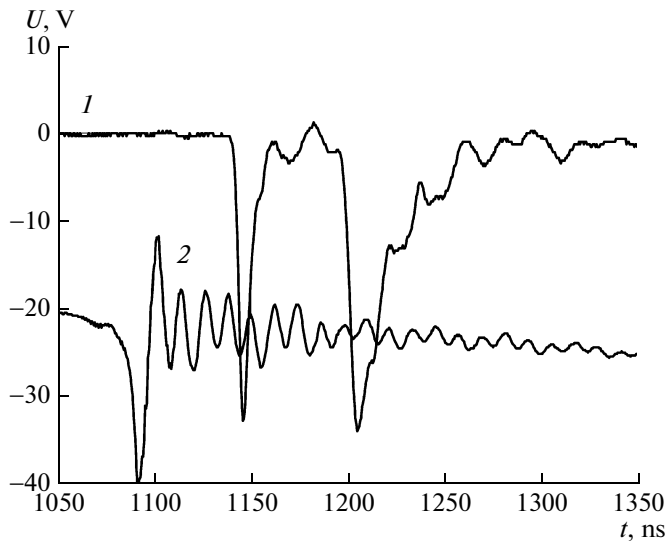


**Fig. 13.** Signal from the scintillation detector (curve 1) and waveform of the current time derivative (curve 2) recorded in a burst of pulses following with a repetition rate of 10 Hz ( $D_2$ , 13 Torr,  $V = 32$  kV, and  $W = 512$  J).

accompanied by a pronounced HXR pulse. In each series of shots, there were 10–20% of HXR and neutron pulses with comparable amplitudes.

In all PMT signals, the HXR pulse was several times shorter than the neutron pulse, but their leading edges were similar. Analysis of the time delays between the HXR and neutron pulses measured at an angle of  $90^\circ$  with respect to the system axis at different distances from the pinch (from 30 to 180 cm) allows us to conclude that, to within measurement errors, neutrons begin to be generated simultaneously with HXR emission. This also makes it possible to determine the velocities of neutrons emitted by the pinch. More exactly, in this way, we can find the velocity of the fastest neutrons detected in the beginning of the pulse. The later part of the neutron pulse can be contributed by neutrons scattered from the HCPG filled with transformer oil, as well as from the floor and walls of the experimental room.

The neutron velocities were measured at an angle of  $90^\circ$  to the chamber axis and along the axis by using the same detector placed at a distance of 132 cm from the center of the anode end. It was assumed that neutrons began to be generated simultaneously with HXR emission. In signals with the well pronounced leading edges of the neutron and X-ray pulses, the time delays between these edges were measured. The averaged (over 10 pulses) time of flight of neutrons emitted at an angle of  $90^\circ$  was found to be  $T_{90} = 56.9 \pm 0.6$  ns, while that of neutrons emitted along the chamber axis was  $T_0 = 53.1 \pm 0.7$  ns. Taking into account the time interval of 4.4 ns required for X-ray photons to travel the distance of 132 cm, we find that the corresponding neutron velocities are  $v_{90} = 2.15 \times 10^9$  cm/s and  $v_0 =$

$2.30 \times 10^9$  cm/s. The “transverse” ( $90^\circ$ ) velocity corresponds to the neutron energy of 2.45 MeV, i.e., the energy of D–D neutrons at a zero deuteron velocity, whereas the “axial” ( $0^\circ$ ) velocity yields an energy of 2.80 MeV. For the interaction of an accelerated deuteron with a deuteron at rest, the latter energy corresponds to the incident deuteron energy of  $\sim 0.1$  MeV.

The neutron yield was measured by means of the activation detector. In the single-pulse mode, the counter was switched on immediately after the discharge. Taking into account that the half-life of silver is 24.5 s and the counter was switched on with a time delay of no longer than 0.5–1 s, the count loss could be neglected against the background of the statistical error. The total neutron yield in a burst of pulses following with a repetition rate of 10 Hz and durations of 1–3 s was measured by the same detector, which was switched on immediately after the end of the burst. For a 3-s-long burst of shots, the count loss (as compared to measurements performed in a single-pulse mode) was at a level of  $\sim 4\%$ .

The distribution of the neutron yield in the burst of shots was measured using the scintillation detector. In most cases, the neutron pulses distinguishable from X-ray pulses in the time of flight turned out to be single and had similar shapes (these experiments were performed with a solid anode end). Hence, under comparable experimental conditions, the burst-averaged amplitude of neutron pulses was proportional to the number of counts of the activation detector divided by the number of shots in the burst. Therefore, to reveal specific features of the neutron yield distribution in one burst, we used the normalized amplitudes of neutron pulses in the scintillation detector signals.

In the experiments carried out with the HCPG, more than 1700 shots were performed and 77 bursts of pulses were recorded. The recorded signals were stored in the internal memory of a LeCroy WJ 324 digital oscilloscope and transferred to a computer by means of a USB flash drive. Using scanning rates of 2 and  $0.5 \mu\text{s}/\text{div}$ , we could record 128 or 512 oscillograms, respectively.

Figures 14 show examples of two bursts of 30 pulses following with a rate of 10 Hz (3-s-long packets) under similar experimental conditions. In burst no. 03-10, the average neutron yield was  $(8.28 \pm 4.75) \times 10^6$  neutrons/pulse (or  $(8.28 \pm 4.75) \times 10^7$  neutrons/s). Good reproducibility of the neutron yield was observed throughout the entire packet. In particular, only in 10% of shots, the neutron yield was below the root-mean-square deviation. Only in one shot (3.3%), the neutron yield was as low as  $0.45 \times 10^6$ , which is 20 times less than the average yield. Moreover, in the parameter range under study (at a packet duration of up to 3 s), no degradation of the neutron yield was observed during the entire burst. In particular, whereas the average neutron yield during the entire burst was

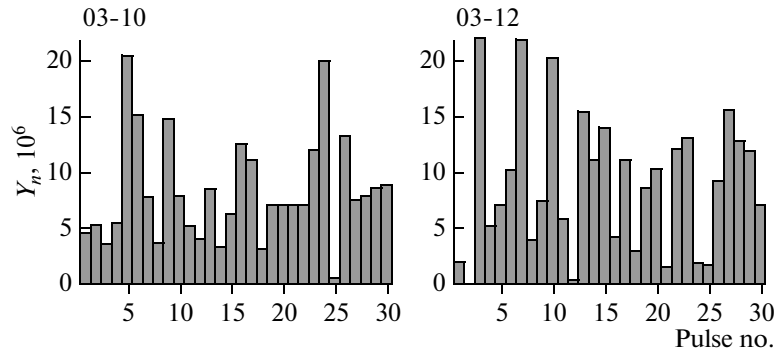


**Fig. 14.** Histograms of the neutron yield distribution in two bursts of pulses following with a repetition rate of 10 Hz under the same experimental conditions ( $I = 82$  kA,  $W = 512$  J,  $P = 13$  Torr,  $D_2$ ). The average neutron flux in burst no. 03-10 is  $8.3 \times 10^7$  n/s, and that in burst no. 03-12 is  $8.6 \times 10^7$  n/s.

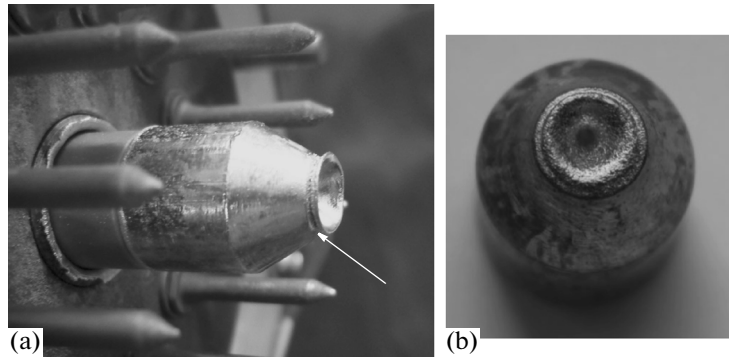


**Fig. 15.** Photographs of (a) the discharge system with an initially plane anode after long-term operation (several tens of bursts) and (b) the eroded anode end.

$8.28 \times 10^6$ , the average neutron yields during the 1st, 2nd, and 3rd seconds were  $8.8 \times 10^6$ ;  $6.8 \times 10^6$ , and  $9.3 \times 10^6$ , respectively.

No dependence of the average and maximum neutron yields on the pulse repetition rate in the range of 0.5–10 Hz was observed. In particular, at a charging voltage of 40 kV and current of 94 kA, the average neutron yield from a burst of 12 pulses following with a repetition rate of 0.5 Hz was  $9 \times 10^6$  neutrons/pulse, whereas at a charging voltage of 35 kV and current of 89 kA, the maximum value of the average neutron yield from a burst of 24 pulses following with a repetition rate of 10 Hz was  $9.4 \times 10^6$  neutrons/pulse. Comparable values were also obtained for the maximum yield:  $2.2 \times 10^7$  neutrons/pulse at a repetition rate of 10 Hz for a discharge energy of 612 J and current of 89 kA and  $1.9 \times 10^7$  neutrons/pulse in the single-pulse mode of HCPG operation (800 J, 94 kA, the interval between pulses of 2 s).

## 6. ANALYSIS OF EXPERIMENTAL RESULTS AND CONCLUSIONS

Thus, a new PF device providing a neutron flux of  $\sim 10^8$  neutron/s when operating in the repetitive mode with a repetition rate of up to 10 Hz and burst duration of up to 3 s has been created. These parameters are advantageous as compared to those achieved in similar existing devices. No degradation of the neutron yield was observed during the entire burst of pulses. The neutron yield somewhat decreases only after long operation of the device (after a large number of bursts) as a result of the wearing of the central part of the anode. Figure 15 shows photographs of the elements of the discharge system with an initially plane anode end after a few hundred discharges. We see a significant erosion of the anode end and the appearance of irregularities that disturb the symmetry of PCS compression, which leads to a reduction in the neutron yield. Special attention should also be paid to the narrow hole with a diameter of  $\sim 1$  mm and depth of  $\sim 3$  mm in the center of the anode. This local hole is a

result of bombardment of the anode by an intense narrow electron beam, which indicates the high quality of current pinching at this device. We also observed the appearance of irregularities at the insulator–anode and insulator–cathode joints, which can also lead to the deterioration of the emission parameters.

Taking into account the results of magnetic probe measurements, it can be stated that the discharge dynamics under conditions of low energy deposition differs insignificantly from that in medium (from a few kJ to a few tens of kJ) and large (from a few hundred kJ to MJ; PF-3, PF-1000, and KPF-4) devices, which agrees with the conclusions made in [21]. The main specific feature is that, for such a small electrode and short discharge duration ( $T/4 \sim 0.7\text{--}0.9 \mu\text{s}$ ), an important role is played by the processes occurring in the initial stage of breakdown and PCS formation, which can take rather a long time. The time remaining after PCS formation may be insufficient to provide focusing at the maximum of the discharge current. The most efficient way to achieve the optimal matching between the dimensions of the discharge system and the parameters of the discharge circuit is to reduce the anode diameter in order to make the energy density on the insulator surface sufficient for the fast formation of the PCS at given parameters of the electric circuit.

The presence of intense HXR fluxes (with photon energies above 200 keV) and the anisotropy of the neutron velocity and neutron flux indicate a substantial contribution of the beam–target mechanism to the neutron generation. It is well known that neutron generation in PF discharges is caused by the interaction of accelerated ions with a plasma target, as well as thermonuclear reactions and processes related to the trapping of accelerated ions in closed magnetic configurations. The integral and spectral parameters of the recorded emission depend on the combination of these mechanisms in particular devices. For example, in large devices, mechanisms related to the ion trapping are dominant. Recent experimental results obtained in these devices indicate a tendency toward saturation of the neutron yield with increasing discharge current, which can be explained, in particular, by the generation of a longitudinal magnetic field preventing efficient compression [42]. High values of the neutron fluxes achieved in our device indicate the possibility of reaching high current contraction and high efficiency of the acceleration processes.

The obtained results (a neutron flux of  $\sim 10^8$  neutrons/s) are very attractive for many practical applications. One of the ways of increasing the neutron flux is to increase the pulse repetition rate above 10 Hz and extend the burst duration. In this stage, operating with bursts of 30 pulses, we did not encounter difficulties related to the overheating of the device elements. However, taking into account the prospects of practical application, it is obvious that the development of

efficient cooling systems is one of the priority lines of further studies. Special attention should also be paid to the development of a new anode design in order to reduce the erosion of the anode end.

## REFERENCES

1. A. Bernard, H. Bruzzone, P. Choj, et al., *J. Moscow Phys. Soc.* **8**, 1 (1998).
2. V. I. Krauz, in *Encyclopedia of Low-Temperature Plasma*, Ed. by V. E. Fortov, Ser. B, Vol. IX-2: *High-Energy Plasmadynamics*, Ed. by A. S. Kingsep (Yanus-K, Moscow, 2007), p. 152 [in Russian].
3. L. Michel, K. H. Schonbach, and H. Fisher, *Appl. Phys. Lett.* **24**, 57 (1974).
4. V. I. Krauz, K. N. Mitrofanov, V. V. Myalton, et al., *Plasma Phys. Rep.* **37**, 742 (2011).
5. M. Scholz, L. Karpinski, V. I. Krauz, et al., *Nukleonika* **57**, 183 (2012).
6. E. A. Andreevich, D. A. Voitenko, V. I. Krauz, et al., *Plasma Phys. Rep.* **33**, 218 (2007).
7. E. C. Hagen, D. Lowe, R. O'Brien, et al., in *Proceedings of the 2013 IEEE Pulsed Power and Plasma Science Conference, San Francisco, CA, 2013*, paper 7B-1.
8. V. I. Krauz, *Plasma Phys. Controlled Fusion* **48**, B221 (2006).
9. L. Soto, *Plasma Phys. Controlled Fusion* **47**, A361 (2005).
10. R. S. Rawat, *Nanosci. Nanotechnol. Lett.* **4**, 251 (2012).
11. M. Krishnan, *IEEE Trans. Plasma Sci.* **40**, 3189 (2012).
12. I. V. Fomenkov, N. Bowering, C. L. Rettig, et al., *J. Phys. D* **37**, 3266 (2004).
13. V. A. Gribkov, V. N. Pimenov, L. I. Ivanov, et al., *IEEE Trans. Plasma Sci.* **30**, 1331 (2003).
14. Z. Y. Pan, R. S. Rawat, J. J. Lin, et al., *J. Plasma Fusion Res. SERIES* **8**, 504.
15. W. P. Singh, M. P. Srivastava, and S. Roy, *J. Plasma Fusion Res. SERIES* **8**, 526 (2009).
16. M. Chernyshova, I. Ivanova-Stanik, L. Karpiński, et al., *Czech. J. Phys.* **56** (Suppl. 1), B237 (2006).
17. Y. Malhotra, S. Roy, M. P. Srivastava, et al., *J. Phys. D* **42**, 155202 (2009).
18. Z. P. Wang, H. R. Yousefi, Y. Nishino, et al., *Phys. Lett. A* **373**, 4169 (2009).
19. O. N. Krokhin, V. Ya. Nikulin, A. A. Tikhomirov, et al., *Nanotekhnika*, No. 13, 52 (2008).
20. B. P. Mikhailov, L. I. Ivanov, I. V. Borovitskaya, et al., *Doklady Phys.* **57**, 61 (2012).
21. L. Soto, C. Pavez, A. Tarifeno, et al., *Plasma Sources Sci. Technol.* **19**, 055017 (2010).
22. P. Silva, J. Moreno, L. Soto, et al., *Appl. Phys. Lett.* **83**, 3269 (2003).
23. L. Soto, P. Silva, J. Moreno, et al., *J. Phys. D* **41**, 205215 (2008).
24. L. Soto, C. Pavez, J. Moreno, et al., *Plasma Sources Sci. Technol.* **18**, 015007 (2009).
25. C. Pavez and L. Soto, *IEEE Trans. Plasma Sci.* **38**, 1132 (2010).

26. V. Rishi, M. V. Roshan, F. Malik, et al., *Plasma Sources Sci. Technol.* **17**, 045020 (2008).
27. A. V. Dubrovsky, V. A. Gribkov, Yu. P. Ivanov, et al., *Nukleonika* **46**, S1, S107 (2001).
28. M. Milanese, R. Moroso, and J. Pouzo, *Eur. Phys. J. D* **27**, 77 (2003).
29. V. Raspa, F. Di Lorenzo, P. Knoblauch, et al., *PMC Phys. A* (2008), doi: 10.1186/1754-0410-2-5, <http://www.physmathcentral.com/content/pdf/1754-0410-2-5.pdf>
30. S. Lee, P. Lee, G. Zhang, et al., *IEEE Trans. Plasma Sci.* **26**, 1119 (1998).
31. V. Rishi, R. S. Rawat, P. Lee, et al., *J. Phys. D* **42**, 235203 (2009).
32. V. Rishi, R. S. Rawat, P. Lee, et al., *J. Fusion Energy* **32**, 32 (2013).
33. B. L. Bures, M. Krishnan, R. E. Madden, and F. Blobner, *IEEE Trans. Plasma Sci.* **38**, 667 (2010).
34. V. Ya. Nikulin, S. N. Polukhin, and A. A. Tikhomirov, *Plasma Phys. Rep.* **31**, 591 (2005).
35. M. Barbaglia, H. Bruzzone, I. Rios, et al., *Plasma Phys. Controlled Fusion* **52**, 032001 (2010).
36. V. I. Krauz, K. N. Mitrofanov, V. V. Myalton, et al., *IEEE Trans. on Plasma Sci.* **38**, 62 (2010).
37. V. I. Krauz, K. N. Mitrofanov, V. V. Myalton, et al., *Plasma Phys. Rep.* **36**, 937 (2010).
38. M. A. Karakin, E. Yu. Khautiev, V. I. Krauz, et al., in *Proceedings of the 15th International Conference on High-Power Particle Beams, St. Petersburg, 2004*, p. 738.
39. V. I. Krauz. *Cand. Sci. (Phys.–Math.) Dissertation (SFTI, Sukhumi, 1988)*, p. 33.
40. G. G. Kanaev, V. R. Kukhta, V. V. Lopatin, et al., *Instrum. Exp. Tech.* **53**, 95 (2010).
41. A. V. Nashilevskiy, G. G. Kanaev, V. I. Krauz, et al., in *Proceedings of the 2011 IEEE Pulsed Power Conference, Chicago, IL, 2011*, p. 923.
42. V. I. Krauz, K. N. Mitrofanov, M. Scholz, et al., *Europhys. Lett.* **98**, 45001 (2012).

*Translated by E. Chernokozhin*